Multistable excitonic Stark effect

Ying Xiong,[1] Mark S. Rudner,[2,3] and Justin C. W. Song[1,*]

[1]*Division of Physics and Applied Physics, School of Physical and Mathematical Sciences, Nanyang Technological University, Singapore 637371*

[2]*Center for Quantum Devices and Niels Bohr International Academy, Niels Bohr Institute, University of Copenhagen, 2100 Copenhagen, Denmark*

[3]*Department of Physics, University of Washington, Seattle, Washington 98195, USA*

(Received 16 September 2020; revised 13 March 2022; accepted 22 April 2022; published 31 May 2022)

The optical Stark effect is a tell-tale signature of coherent light–matter interaction in excitonic systems, wherein an irradiating light beam tunes exciton transition frequencies. Here we show that, when excitons are placed in a nanophotonic cavity, the excitonic Stark effect can become highly nonlinear, exhibiting multivalued and hysteretic Stark shifts that depend on the history of the irradiating light. This multistable Stark effect (MSE) arises from feedback between the cavity mode occupation and excitonic population mediated by the Stark-induced mutual tuning of the cavity and excitonic resonances. Strikingly, the MSE manifests even for very dilute exciton concentrations and can yield discontinuous Stark shift jumps of order meV. We expect that the MSE can be realized in readily available transition metal dichalcogenide excitonic systems placed in planar photonic cavities at modest pump intensities. This phenomenon can provide new means to engineer coupled states of light and matter that can persist even in the single exciton limit.

DOI: 10.1103/PhysRevResearch.4.023168

I. INTRODUCTION

Strong light–matter interaction can provide a versatile platform for dynamically controlling quantum matter [1]. A striking example is the excitonic optical Stark effect [2–5]: Off-resonant irradiation of an excitonic system, with frequency below the exciton transition energy, continuously blue-shifts the exciton transition to higher frequencies as the light intensity increases [4–8]. In contrast with the fixed Rabi splitting found for polaritons, which is independent of the intensity of light [9–11], the optical Stark effect is linear in the irradiation intensity. This dependence grants on-demand tunability of excitonic properties. On a fundamental level, the Stark effect arises from a variety of origins, including the underlying fermionic nature of the exciton's constituents as well as Coulomb interactions [6,12]. In transition metal dichalcogenides (TMDs), Stark shifts are furthermore sensitive to light polarization, thereby enabling direct control over the valley excitons necessary for valley optoelectronics [8,13,14].

Here we propose that the optical Stark effect can take on a markedly different character when an excitonic system is placed in a nanophotonic cavity (Fig. 1, inset). In this setting, the Stark shift becomes a dynamical variable, with the cavity field taking on the role of the irradiating field that shifts the excitonic levels. In particular, when the excitonic and cavity modes are simultaneously pumped with separate driving fields, the optical Stark effect can become multistable, exhibiting a hysteretic Stark shift that depends on the history of the optical drive. As we explain below and indicate in Fig. 1, this multistable Stark effect (MSE) arises due to a Stark-induced mutual tuning; the excitonic transition frequency (right panel) is sensitive to the cavity mode occupation, while the cavity resonance (left panel) is sensitive to the exciton population. When applied exciton and cavity driving fields are detuned from their respective bare transition frequencies, the mutual tuning sets up a feedback that shifts the exciton and cavity transition frequencies into resonance with their respective drives (dashed to solid lines, Fig. 1). This feedback leads to large nonlinearities that result in the MSE, which, as we discuss below, can persist even in very dilute systems.

The MSE features discontinuous transitions between multiple distinct steady states of the combined cavity-exciton system and can exhibit large discontinuous Stark shift jumps of order meV. Indeed, we find that the exciton population can take on multiple steady-state values [Fig. 2(a)] with a hysteretic behavior that is controlled by a weak cavity drive far detuned from the original exciton resonance. Further, the magnitude of the Stark shift jump from one stable state to another can be directly tuned by the drive that pumps the excitonic population. These mechanisms provide *in situ* means of tailoring the switching behavior in the exciton/cavity system.

In what follows, we will first demonstrate the origin of the MSE in a simple illustrative setup of a single exciton emitter coupled to a cavity mode. We then extend our analysis to a monolayer TMD (e.g., WS_2) hosting a large number of degenerate and delocalized excitonic states coupled to a photonic crystal cavity. We show that the MSE can be achieved when

*Corresponding author: justinsong@ntu.edu.sg

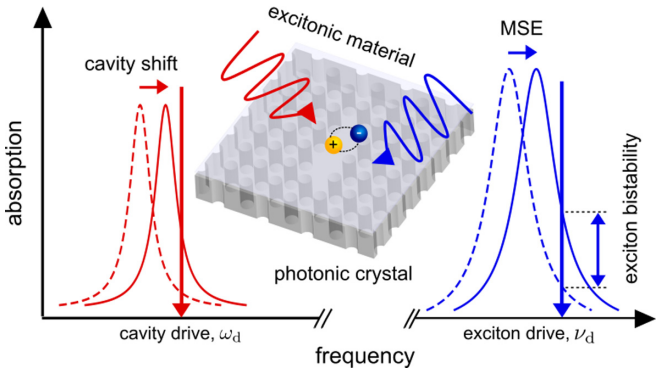

FIG. 1. Mutual tuning of exciton (right panel) and cavity (left panel) transitions induced by the optical Stark effect, wherein the exciton transition frequency is sensitive to the cavity mode occupation (and vice versa). When the excitons and the cavity mode are simultaneously pumped by their individual driving fields (downward arrows indicate the corresponding pump frequencies), the exciton and cavity transitions can shift into resonance with their drives (from dashed to solid curves). These population-induced shifts generate the feedback loop that gives rise to the MSE. (Inset) A two-dimensional excitonic material such as a TMD can be readily layered on top of a planar nanophotonic cavity formed by a photonic crystal defect to achieve the conditions for realizing the MSE.

the valley excitons and the cavity mode are both driven by individual circularly polarized light fields with realistic TMD parameters, see below. We expect that the MSE can be realized in TMDs on currently available high quality factor planar photonic cavities [15–18] (Fig. 1, inset) even at moderate optical drive strengths of tens of kW/cm^2. As we argue below, this MSE platform provides new means of constructing hysteretic, nonlinearly coupled states of light and matter that can, in principle, persist even at the single exciton limit.

II. STARK-INDUCED MUTUAL TUNING AND NONLINEARITY

The key to achieving the MSE is the nonlinearity mediated by strong coupling between cavity photon modes and excitons. As we now explain, this nonlinearity in the cavity-exciton system can arise directly through the Stark effect. As a simple and clear illustration of the MSE, we first focus on a single localized excitonic mode interacting with a single discrete cavity mode of a single polarization (e.g., that of a localized exciton mode in a quantum dot). We will discuss the MSE for delocalized excitons in a large TMD sample coupled to a discrete cavity mode later in the text.

We model the localized exciton mode as a simple two-level system with bare resonance angular frequency $\nu^{(0)}$; we denote the ground state (no exciton) by $|P=0\rangle$ and the excited state (exciton present) by $|P=1\rangle$. The cavity photon mode has angular frequency $\omega^{(0)}$. In the dispersive limit, the dynamics of the system are described by the Hamiltonian $H = H_X + H_0 + H_{\rm int}$ with (setting $\hbar = 1$ here and throughout, unless otherwise stated):

$$H_X = \nu^{(0)}\hat{P}, \quad H_0 = \omega^{(0)}a^\dagger a, \quad H_{\rm int} = Va^\dagger a\hat{P}, \tag{1}$$

where $a^\dagger$ is the creation operator for the cavity photon mode, and $\hat{P} = s^z + \mathbb{1}/2$ counts the exciton population via $\hat{P}|P\rangle = P|P\rangle$, where $\mathbb{1}$ is the 2×2 identity matrix and $s^z = \sigma^z/2$, where σ^z is the third Pauli matrix.

The last term in Eq. (1) encodes a dispersive coupling, V, between the excitons and the cavity photons that is valid for $V \ll |\nu^{(0)} - \omega^{(0)}|, \omega^{(0)}, \nu^{(0)}$. In this limit, the magnitude of V can be controlled directly through engineering of the microcavity mode profile and its detuning from the exciton resonance. Throughout this work we will consider $V > 0$ and treat V as a phenomenological material-dependent parameter. We note that this simple phenomenological model of a dispersive exciton-photon coupling captures the essential feature of the exciton Stark shift—its dependence on the intensity of light—that is widely seen in experiments [8,13,14]. For a detailed discussion of the dispersive coupling strength in an extended excitonic system and realistic parameter estimates in a TMD/cavity structure, see later sections.

Crucially, through the dispersive coupling, both the exciton and the cavity photon resonances are mutually dependent on the other's occupation. For a state with m cavity photons present and excitonic state $P = \{0, 1\}$, the (cavity-dressed) exciton and (exciton-dressed) cavity photon resonance angular frequencies, $\tilde{\nu}(m)$ and $\tilde{\omega}(P)$, respectively, are given by:

$$\tilde{\nu}(m) = \nu^{(0)} + Vm, \quad \tilde{\omega}(P) = \omega^{(0)} + VP. \tag{2}$$

The excitonic resonance $\tilde{\nu}(m)$ experiences a blue shift away from its bare resonance frequency that is proportional to the photon number in the cavity—the optical Stark effect [3,4,6,8]. We characterize this by the excitonic Stark shift: $\delta E \equiv \tilde{\nu}(m) - \nu^{(0)} = Vm$. Similarly, the cavity photon resonance frequency $\tilde{\omega}(P)$ also depends on the occupation of the excitonic state, shifting as P changes. The mutual tuning of exciton and cavity photon transitions exhibited in Eq. (2) provides a natural means of feedback, and as we now discuss, gives rise to nonlinear dynamical phenomena in the system. Indeed, this Stark-induced mutual tuning (and the nonlinear dynamical phenomena it enables) is not dependent on the simple two-level structure of Eq. (1); as we will see later in the text, Stark-induced mutual tuning persists even in a bosonic framework.

III. MSE AND CAVITY-EXCITON STEADY STATES

To demonstrate the MSE, we consider an exciton-photon microcavity system with laser drives at angular frequencies ν_d and ω_d. These fields pump the excitonic and cavity photon modes, respectively. This selectivity can be achieved by choosing ν_d and ω_d to be slightly detuned from $\tilde{\nu}(0)$ and $\tilde{\omega}(0)$, respectively, with their individual detunings much smaller than $|\nu^{(0)} - \omega^{(0)}|$.

In the presence of these laser driving fields, the Hamiltonian becomes $\mathcal{H}(t) = H + H_X^{(d)}(t) + H_0^{(d)}(t)$, with

$$H_X^{(d)}(t) = \frac{F_X}{2}(e^{-i\nu_d t}\sigma^+ + \text{H.c.}),$$
$$H_0^{(d)}(t) = \frac{F_0}{2}(e^{-i\omega_d t}a^\dagger + \text{H.c.}), \tag{3}$$

where F_X and F_0 are the drive amplitudes, and $\sigma^+ = (\sigma^x + i\sigma^y)/2$, where $\sigma^{x,y}$ are the x, y Pauli matrices. In anticipation

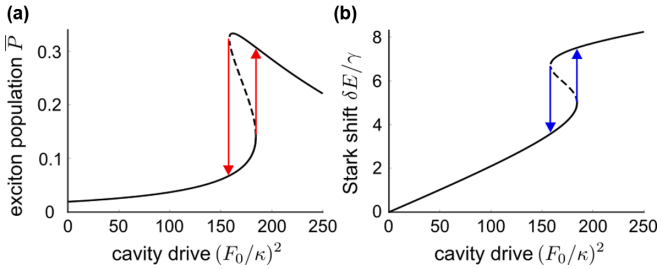

FIG. 2. A single excitonic emitter coupled to a cavity can display bistable and hysteretic steady states of the (a) exciton and (b) cavity photon populations (reflected in the Stark shift, δE). The steady states are obtained by solving Eqs. (8) and (9); the thick solid lines indicate the stable solutions, and the thin dashed lines indicate the unstable solutions. Illustrative dimensionless parameters used: $F_X/\gamma = 2$, $V/\gamma = 0.25$, $\nu^d - \nu(0) = 7\gamma$, $\omega^d - \tilde{\omega}(0) = 1.5\kappa$, and $\gamma/\kappa = 10$.

of making a rotating wave approximation below, we have discarded counter-rotating terms in Eq. (3).

To explicitly demonstrate the MSE, we track the exciton and cavity photon populations in the driven system in the presence of Markovian dissipation that accounts for exciton relaxation (recombination) and cavity photon loss. As a first step, we transform into a frame that corotates with the drives using $U(t) = \exp(-i\omega_d t\, a^\dagger a - i\nu_d t\, \hat{P})$. In the rotating frame, the system evolves according to the (static) Hamiltonian $\tilde{\mathcal{H}} = \tilde{H}_X + \tilde{H}_0 + \tilde{H}_{\rm int}$, with $\tilde{H}_X = (\nu^{(0)} - \nu_d)\hat{P} + F_X\sigma^x/2$, and $\tilde{H}_0 = (\omega^{(0)} - \omega_d)a^\dagger a + F_0(a^\dagger + a)/2$. The interaction $\tilde{H}_{\rm int} = Va^\dagger a\hat{P}$ does not change under the transformation.

Using the rotating-frame Hamiltonian $\tilde{\mathcal{H}}$, we take the density matrix of the composite exciton and cavity system (in the rotating frame), $\tilde{\rho}(t)$, to evolve according to the master equation

$$\partial_t\tilde{\rho} = i[\tilde{\rho}(t), \tilde{H}_0 + \tilde{H}_X + \tilde{H}_{\rm int}] + \mathcal{I}_X[\tilde{\rho}(t)] + \mathcal{I}_0[\tilde{\rho}(t)], \quad (4)$$

where $\mathcal{I}_X[\tilde{\rho}] = \gamma(2\sigma^-\tilde{\rho}\sigma^+ - \sigma^+\sigma^-\tilde{\rho} - \tilde{\rho}\sigma^+\sigma^-)$ accounts for recombination of the exciton, with rate γ, and $\mathcal{I}_0[\tilde{\rho}] = \kappa(2a\tilde{\rho}a^\dagger - a^\dagger a\tilde{\rho} - \tilde{\rho}a^\dagger a)$ describes losses in the microcavity photon mode with rate κ. The interaction $\tilde{H}_{\rm int} \neq 0$ couples the cavity and exciton subsystems by the mutual tuning of their transition frequencies as in Eq. (2).

While Eq. (4) can generically encode a variety of complex dynamical regimes of the composite system, as we now discuss, a large separation in the cavity and exciton decay timescales enables direct evaluation of the MSE steady states (cf. Ref. [19] for a general discussion). Indeed, the regime wherein the excitonic system relaxes far faster than the cavity photon system can be readily achieved in many exciton-cavity setups; see estimate below. Physically, this separation of timescales means that the reduced density matrix of the excitonic system $\tilde{\rho}_X(t) \equiv {\rm Tr}_0\,\tilde{\rho}(t)$ rapidly reaches a quasistationary state over a time that is short compared with the characteristic evolution timescale of the cavity photon; here ${\rm Tr}_0$ [${\rm Tr}_X$] denotes the partial trace over photonic [excitonic] degrees of freedom. On the timescale of excitonic relaxation, the cavity state $\tilde{\rho}_0(t) \equiv {\rm Tr}_X\tilde{\rho}(t)$ can be treated as quasistatic, allowing the formation of an excitonic steady state that depends parametrically on $\tilde{\rho}_0$. On the timescale that the cavity state $\tilde{\rho}_0(t)$ evolves, $\tilde{\rho}_X(t)$ maintains a quasistationary state that adiabatically follows the slow evolution of $\tilde{\rho}_0(t)$.

Using this separation of timescales, in describing the time evolution of the exciton and cavity photons we adopt a mean-field decoupling [19] of Eq. (4) by replacing the cavity-exciton coupling by its mean-field averages ${\rm Tr}_0[\tilde{\rho}(t)\tilde{H}_{\rm int}] \to V\langle m(t)\rangle\hat{P}$ and ${\rm Tr}_X[\tilde{\rho}(t)\tilde{H}_{\rm int}] \to Va^\dagger a\langle\hat{P}(t)\rangle$, where $\langle\hat{P}(t)\rangle \equiv {\rm Tr}[\hat{P}\tilde{\rho}_X(t)]$ and $m(t) \equiv {\rm Tr}[a^\dagger a\tilde{\rho}_0(t)]$. This mean-field decoupling is justified in the semiclassical regime where the photon number in the cavity is large and fluctuations are small [19]. With this mean-field decoupling, the (rotating frame) exciton and cavity density matrices $\tilde{\rho}_X(t)$ and $\tilde{\rho}_0(t)$, respectively, evolve according to:

$$\partial_t\tilde{\rho}_X(t) = i[\tilde{\rho}_X(t), \tilde{H}_X + V\langle m(t)\rangle\hat{P}] + \mathcal{I}_X[\tilde{\rho}_X(t)], \quad (5)$$

$$\partial_t\tilde{\rho}_0(t) = i[\tilde{\rho}_0(t), \tilde{H}_0 + Va^\dagger a\langle\hat{P}(t)\rangle] + \mathcal{I}_0[\tilde{\rho}_0(t)]. \quad (6)$$

The exciton population dynamics can be obtained by directly evaluating the elements of $\tilde{\rho}_X(t)$ in Eq. (5) to obtain effective Bloch equations. Writing $\langle s^i(t)\rangle \equiv {\rm Tr}\,[s^i\tilde{\rho}_X(t)]$ where $s^i = \sigma^i/2$ for $i = x, y, z$, and noting ${\rm Tr}\,[\tilde{\rho}_X(t)] = 1$, we obtain

$$\begin{aligned}
\partial_t\langle s^x(t)\rangle &= \delta\nu(t)\langle s^y(t)\rangle - \gamma\langle s^x(t)\rangle,\\
\partial_t\langle s^y(t)\rangle &= -F_X\langle s^z(t)\rangle - \delta\nu(t)\langle s^x(t)\rangle - \gamma\langle s^y(t)\rangle, \quad (7)\\
\partial_t\langle s^z(t)\rangle &= F_X\langle s^y(t)\rangle - 2\gamma(\langle s^z(t)\rangle + 1/2),
\end{aligned}$$

where $\delta\nu(t) = \nu_d - \tilde{\nu}[\langle m(t)\rangle]$. We solve for the excitonic (quasi)-steady state by setting the three equations above equal to zero, and assuming that the cavity mode occupation $\langle m(t)\rangle = m$ is fixed. We thus obtain the (quasi)-steady-state population of the excitonic mode as a function of the cavity occupation, m:

$$\overline{P}(m) = \overline{\langle s^z\rangle} + \frac{1}{2} = \frac{F_X^2/2}{F_X^2 + 2[\gamma^2 + (\nu_{\rm d} - \tilde{\nu}(m))^2]}, \quad (8)$$

where $\overline{\langle s^z\rangle}$ is the time independent steady-state solution of Eq. (7). As is evident from Eq. (8), the steady-state excitonic population depends both on the excitonic drive strength, F_X, and parametrically on the cavity population through the stark-shifted exciton resonance, $\tilde{\nu}(m)$. We note that the exciton population is always zero in the absence of exciton drive (i.e., $F_X = 0$), and we will see later that we need both the exciton drive and the cavity drive to achieve mutual tuning and multistability.

The steady-state cavity population can be obtained heuristically by first considering the familiar expression for the average population of a driven cavity mode with a fixed resonance frequency, ω: $\bar{m} = (F_0^2/4)/\{\kappa^2 + (\omega_{\rm d} - \omega)^2\}$. Due to the Stark-induced mutual tuning described above, the cavity resonance frequency changes with the exciton population; see Eq. (2). As a result, we replace $\omega \to \tilde{\omega}[\overline{P}(m = \bar{m})]$ to yield a self-consistency relation for the cavity mode population:

$$\bar{m} = \left(F_0^2/4\right)/\{\kappa^2 + (\omega_{\rm d} - \tilde{\omega}[\overline{P}(\bar{m})])^2\}. \quad (9)$$

We note that this heuristically obtained self-consistency relation agrees with results obtained through careful analysis of the evolution of the full density matrix of the joint system in

the regime $\kappa/\gamma \ll 1$ and $V^2/\gamma \ll \kappa$ [19]. The steady-state cavity occupation thus depends on the steady-state exciton population through its mutually tuned cavity transition in Eq. (2). For a detailed discussion of nonadiabatic effects and switching near bifurcation points, see, e.g., Ref. [19].

We now explicitly exhibit the multistability described by Eqs. (8) and (9). Choosing drive frequencies slightly blue detuned from the bare exciton and cavity resonances (see Fig. 2 and caption for parameter values), Eqs. (8) and (9) yield multiple solutions for $\overline{P}$ as a function of F_0 (for all other parameters held fixed in this regime). These multiple steady states arise from the MSE, as evidenced by the jumps of the Stark shift δE (on the order of the exciton decay rate γ) displayed in Fig. 2(b).

Within the bistable regime, two distinct stable steady-state solutions for $\overline{P}$ and δE exist for the same drive parameters (solid lines). This enables a hysteretic behavior of the excitonic system that depends on the history of the optical drive. Indeed, as F_0 increases from zero (forward sweep), $\overline{P}$ (as well as $\bar{m}$) jumps to the upper branch of solutions (upward arrow) at a forward threshold amplitude. However, when F_0 is then decreased (reverse sweep), both $\overline{P}$ (and δE) jump to the lower branch of solutions (downward arrow) at a distinct reverse threshold amplitude. This hysteresis enables the system to operate as an optically controlled "exciton switch" with "off" and "on" states as the lower and upper branches.

Strikingly, this excitonic hysteresis can occur even for the extreme case of a single excitonic mode (described above), in sharp contrast with other types of excitonic nonlinearities that are only induced at high exciton density and large exciton–exciton interactions [20]. As we will see below, in the presence of multiple excitonic modes/emitters, this unusual property enables the MSE to manifest in dilute exciton gases. We note that such driven modes are a prime venue for realizing nonlinear behavior in a wide variety of parameter regimes; see, e.g., Ref. [21] where nonlinearities in circuit QED were analyzed in the regime of large $V > \kappa, \Gamma$.

IV. MSE IN TMDS

Having exhibited the MSE mechanism for a single excitonic emitter, we now discuss the MSE in readily available two-dimensional excitonic systems. A natural class of candidate materials are the atomically thin TMDs, which possess room-temperature stable excitons and large Stark effects [8,13,14] and can be easily integrated with planar photonic crystal cavities, as in the inset of Fig. 1. Here we will focus on the zero center of mass momentum (COMM) excitons in a single valley, where excitons obey circular polarization selection rules [22–27]. By driving both the TMD and the cavity mode with individual circularly polarized driving fields of fixed handedness, only circularly polarized cavity photons and excitons in the corresponding valley will be excited.

To describe the MSE in TMDs, we consider an extended TMD layer placed on top of a photonic cavity formed by a defect in a planar photonic crystal; see Fig. 1 inset. We first note that the TMD excitonic mode at $\nu^{(0)}$ can have a large effective degeneracy $\mathcal{N}$. This degeneracy accounts for excitons at distinct exciton center of mass spatial coordinates; these degenerate exciton emitters can form plane-wave superpositions that lead to delocalized excitonic modes [28–30]. Importantly, the modes with zero COMM interact coherently (in phase) with the same cavity photonic mode [28–30] (with a wavelength of a few hundred nanometers); similarly, for exciton pumping fields that have large wavelengths of order several hundred nanometers, multiple excitonic emitters can be driven in phase with each other. As such, in describing the TMD layer excitonic-cavity system, we replace $\hat{P} \to \hat{P}_{\rm tot} = \sum_j \hat{P}_j$ in the Hamiltonian Eq. (1), as well as $\sigma^{+,-} \to s^{+,-}_{\rm tot} = \sum_j \sigma^{+,-}_j$ in Eq. (3), where the sum over j runs over each of the $j = 1, \ldots, \mathcal{N}$ degenerate excitonic emitters. Similarly, $\tilde{\omega}(P_{\rm tot}) \to \tilde{\omega} = \omega^{(0)} + V P_{\rm tot}$ in Eq. (2) where $P_{\rm tot} = 0, 1, 2, \cdots$ are eigenvalues of $\hat{P}_{\rm tot}$. Since all the emitters interact with the same cavity photon mode, $\tilde{\nu}(m)$ in Eq. (2) remains unchanged. Importantly, in the regime of low-excitation density which we focus on, this treatment produces the same results as a bosonic approach; see the Supplemental Material [31].

We follow a similar procedure and use the separation of timescales as discussed above for tracking the exciton and cavity photon populations (see the Supplemental Material for full details [31]). As we will discuss below, in the coupled system of a monolayer TMD embedded in a photonic crystal, we will work with (realistic) choices of exciton (Γ) and cavity (κ) linewidths and exciton-photon coupling constant V with $\kappa/\Gamma \ll 1$ and $V^2/\Gamma \ll \kappa$ such that the mean-field decoupling is valid. In so doing, we take a spin-coherent-state ansatz so that the dynamics of the multiple emitter system can be analyzed in terms of the dynamics of a giant spin $\mathbf{s}_{\rm tot} = s^x_{\rm tot}\hat{\mathbf{x}} + s^y_{\rm tot}\hat{\mathbf{y}} + s^z_{\rm tot}\hat{\mathbf{z}}$, where $s^{x,y,z}_{\rm tot} = \sum_i s^{x,y,z}_i$ is summed over the excitonic emitters. For fixed cavity occupation m we obtain the steady-state exciton population in the extended system (see the Supplemental Material [31]) as

$$\overline{P}_{\rm tot} = \frac{\mathcal{N} F_X^2/2}{F_X^2 + 2(\Gamma^2 + [\nu_d - \nu(m)]^2)}, \tag{10}$$

where Γ is the exciton recombination rate (for the zero COMM excitons) in the extended TMD system; we note, parenthetically, that this rate can be estimated from the recombination rate γ of a single localized exciton emitter as $\Gamma \sim \mathcal{N}\gamma$ [28–30]. In obtaining Eq. (10) we have taken a large degeneracy $\mathcal{N} \gg 1$ as well as focused on the low-excitation regime. We note in the low-density/low-excitation regime, $F_X \ll \Gamma, \nu_d, \tilde{\nu}$, Eq. (10) reproduces $\overline{P}_{\rm tot}$ obtained from a bosonic treatment; see the Supplemental Material [31]. Indeed, both approaches produce a $\overline{P}_{\rm tot}$ that is described by a Lorentzian resonance peak that is tuned by the cavity photon mode, m, as illustrated schematically in Fig. 1. As we will see below, it is this mutual tuning of resonance peaks that is critical for MSE.

Before we exhibit the MSE in TMD systems, we first discuss the parameters for the cavity-exciton system. We note that the excitonic mode degeneracy $\mathcal{N}$ can be large and can range from $\mathcal{N} \sim 10^2 - 10^4$ [28]; this arises from the large number of excitonic modes that can interact coherently within a single wavelength of either the cavity photon mode or the exciton drive [28–30]. An estimate of $\mathcal{N}$ can be obtained

from the ratio of the mode area of the photonic mode (the square of its wavelength) and the effective size of an exciton (the square of its Bohr radius) [30]. Further, recombination times for zero COMM excitons in typical monolayer TMDs can range from $\Gamma^{-1} \sim 0.5$ to a few picoseconds [32–36], whereas cavity relaxation times can be as long as tens to a hundred picoseconds [15–18]. As a result, $\kappa \ll \Gamma$, justifying the separation of timescales and the mean-field decoupling approach we have used to describe the MSE. Last, strong light–matter interaction in monolayer TMDs [8,13] can lead to values of the dispersive coupling V up to 0.5 meV; see the Supplemental Material for a detailed estimate [31]. In the plots we have chosen $V \approx 0.061$ meV, which is directly obtained from experimental measurements at photon-exciton detuning $\Delta_{\text{cav}} = 120$ meV for the TMD system monolayer WS_2 [8].

Solving Eq. (10) together with Eq. (9) yields an excitonic multistability and the MSE, as shown in Fig. 3. With realistic parameters for monolayer WS_2 and photonic crystal cavities, discontinuous jumps in the excitonic Stark shift can be readily achieved by moderate exciton drive intensities of order kW/cm^2 and moderate cavity drives of order of tens of kW/cm^2.

Interestingly, distinct regimes of multistability can be accessed; at low exciton drive strength, a bistable MSE manifests (as cavity drive is swept) whereas larger exciton drives display tristabilities [see Fig. 3(a)]. Indeed, the MSE displays hysteretic behavior as either exciton or cavity drives are swept, with Figs. 3(b) and 3(c) displaying sizable discontinuities of δE of order meV. We note that together with multistable δE shown in Fig. 3, the exciton population $\overline{P}_{\text{tot}}$ similarly exhibits multistability and hysteresis (see also Fig. 2). While we have focused on the MSE and its concomitant excitonic multistability, multiple stable states of the cavity mode (so-called "optical multistability" characterized by distinct steady-state values of $\bar{m}$) can also arise via the MSE. [Note that in Fig. 2(b), δE is directly proportional to the cavity photon occupation.] This effect is similar to dispersive optical multistability in highly nonlinear optical media [37–42] and may provide new means for controlling optical states.

Strong light–matter coupling enables the MSE to persist even in dilute exciton systems. Indeed, we find in Fig. 3 that a MSE manifests for a steady-state excitonic population on the order of $\overline{P}_{\text{tot}} \sim 1$; see the Supplemental Material [31]. This indicates that the MSE occurs even as approximately one exciton is excited in the entire photonic cavity (corresponding to a low exciton density of order 10^{10} cm^{-2}). This enables the MSE to persist to low exciton densities that are challenging to realize in other mechanisms for bistability [43,44]. Looking forward, we anticipate that MSE-controlled excitons may provide new tools to tune the properties and the collective dynamics of dilute excitonic systems and new quantum materials [1,45–47].

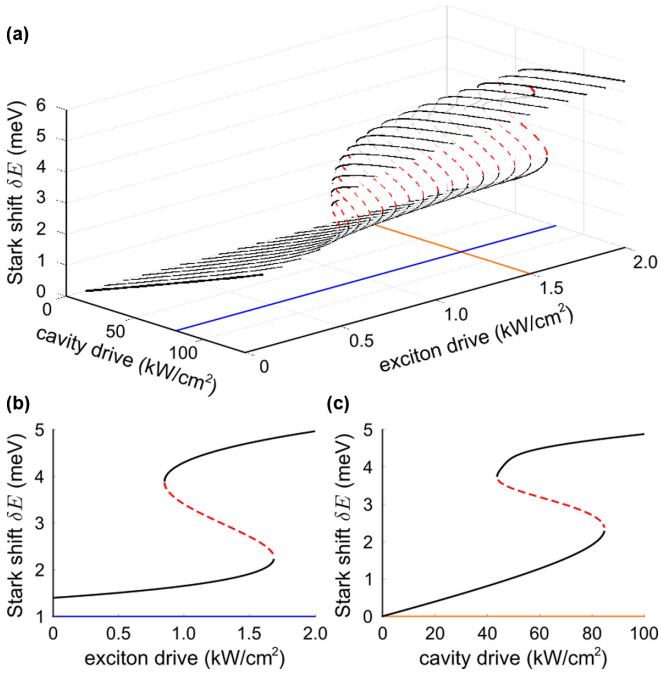

FIG. 3. (a) MSE shift δE of the excitonic system in a monolayer TMD coupled to a cavity obtained from Eqs. (9) and (10) displaying multiple steady states (bistable [low exciton drive] and then tristable [larger exciton drive]) and discontinuous δE jumps. Panel (b) shows a line cut of δE as a function of exciton drive at a fixed cavity drive of 80 kW/cm^2 [as indicated by the blue line in (a)]. Panel (c) displays δE as a function of cavity drive at a fixed exciton drive of 1.5 kW/cm^2 [as indicated by the orange line in (a)]. Solid lines indicate stable solutions, whereas dashed lines indicate unstable states. Here we used parameters $\Gamma = 1$ meV, $\nu_d - \nu(0) = 4$ meV, dispersive coupling $V \approx 0.061$ meV [8], $\kappa = 0.1$ meV, $\mathcal{N} = 1000$, and $\omega_d - \omega(0) = 0.2$ meV; see the Supplemental Material for detailed estimates and discussion of parameters [31].

ACKNOWLEDGMENTS

J.C.W.S. acknowledges support from the Ministry of Education, Singapore under its MOE AcRF Tier 3 Award No. MOE2018-T3-1-002 and a Nanyang Technological University start-up grant (NTU-SUG). M.R. gratefully acknowledges the support of the Villum Foundation, and the European Research Council (ERC) under the European Union Horizon 2020 Research and Innovation Programme (Grant Agreement No. 678862).

[1] D. N. Basov, R. D. Averitt, and D. Hsieh, Towards properties on demand in quantum materials, Nat. Mater. **16**, 1077 (2017).

[2] A. Mysyrowicz, D. Hulin, A. Antonetti, A. Migus, W. T. Masselink, and H. Morkoc, "Dressed Excitons" in a Multiple-Quantum-Well Structure: Evidence for an Optical Stark Effect with Femtosecond Response Time, Phys. Rev. Lett. **56**, 2748 (1986)

[3] S. Schmitt-Rink and D. S. Chemla, Collective Excitations and the Dynamical Stark Effect in a Coherently Driven Exciton System, Phys. Rev. Lett. **57**, 2752 (1986).

[4] S. H. Autler and C. H. Townes, Stark effect in rapidly varying fields, Phys. Rev. **100**, 703 (1955).

[5] A. Von Lehmen, D. S. Chemla, J. E. Zucker, and J. P. Heritage, Optical Stark effect on excitons in GaAs quantum wells, Opt. Lett. **11**, 609 (1986).

[6] M. Combescot, Polariton versus optical stark effect: An old concept revisited, Solid State Commun. **74**, 291 (1990).

[7] A. Hayat, C. Lange, L. A. Rozema, A. Darabi, H. M. van Driel, A. M. Steinberg, B. Nelsen, D. W. Snoke, L. N. Pfeiffer, K. W. West *et al.*, Dynamic Stark Effect in Strongly Coupled Microcavity Exciton Polaritons, Phys. Rev. Lett. **109**, 033605 (2012).

[8] E. J. Sie, J. W. McIver, Y. H. Lee, L. Fu, J. Kong, and N. Gedik, Valley-selective optical Stark effect in monolayer WS_2, Nat. Mater. **14**, 290 (2015).

[9] J. J. Hopfield, Theory of the contribution of excitons to the complex dielectric constant of crystals, Phys. Rev. **112**, 1555 (1958).

[10] C. Weisbuch, M. Nishioka, A. Ishikawa, and Y. Arakawa, Observation of the coupled exciton-photon mode splitting in a semiconductor quantum microcavity, Phys. Rev. Lett. **69**, 3314 (1992).

[11] X. Liu, T. Galfsky, Z. Sun, F. Xia, E. Lin, Y. Lee, S. Kéna-Cohen, and V. M. Menon, Strong lightmatter coupling in two-dimensional atomic crystals, Nat. Photonics **9**, 30 (2015).

[12] M. Combescot and R. Combescot, Excitonic Stark Shift: A Coupling to "Semivirtual" Biexcitons, Phys. Rev. Lett. **61**, 117 (1988).

[13] E. J. Sie, C. H. Lui, Y. H. Lee, L. Fu, J. Kong, and N. Gedik, Large, valley-exclusive Bloch-Siegert shift in monolayer WS_2, Science **355**, 1066 (2017).

[14] C.-K. Yong *et al.*, Biexcitonic optical Stark effects in monolayer molybdenum diselenide, Nat. Phys. **14**, 1092 (2018).

[15] J. Zhou, J. Zheng, Z. Fang, P. Xu, and A. Majumdar, Ultralow mode volume on-substrate silicon nanobeam cavity, Opt. Express **27**, 30692 (2019).

[16] R. Miura, S. Imamura, R. Ohta, A. Ishii, X. Liu, T. Shimada, S. Iwamoto, Y. Arakawa, and Y. K. Kato, Ultralow mode-volume photonic crystal nanobeam cavities for high-efficiency coupling to individual carbon nanotube emitters, Nat. Commun. **5**, 5580 (2014).

[17] T. Asano, Y. Ochi, Y. Takahashi, K. Kishimoto, and S. Noda, Photonic crystal nanocavity with a Q factor exceeding eleven million, Opt. Express **25**, 1769 (2017).

[18] X. Yang, A. Ishikawa, X. Yin, and X. Zhang, Hybrid Photonic-Plasmonic Crystal Nanocavities, ACS Nano **5**, 2831 (2011).

[19] Z. Maizelis, M. Rudner, and M. I. Dykman, Vibration multistability and quantum switching for dispersive coupling, Phys. Rev. B **89**, 155439 (2014).

[20] A. Baas, J. Ph. Karr, H. Eleuch, and E. Giacobino, Optical bistability in semiconductor microcavities, Phys. Rev. A **69**, 023809 (2004).

[21] Th. K. Mavrogordatos, G. Tancredi, M. Elliott, M. J. Peterer, A. Patterson, J. Rahamim, P. J. Leek, E. Ginossar, and M. H. Szymaska, Simultaneous Bistability of a Qubit and Resonator in Circuit Quantum Electrodynamics, Phys. Rev. Lett. **118**, 040402 (2017).

[22] G. Wang, A. Chernikov, M. M. Glazov, T. F. Heinz, X. Marie, T. Amand, and B. Urbaszek, Colloquium: Excitons in atomically thin transition metal dichalcogenides, Rev. Mod. Phys. **90**, 021001 (2018).

[23] A. M. Jones, H. Yu, N. J. Ghimire, S. Wu, G. Aivazian, J. S. Ross, B. Zhao, J. Yan, D. G. Mandrus, Di Xiao *et al.*, Optical generation of excitonic valley coherence in monolayer WSe_2, Nat. Nanotechnol. **8**, 634 (2013).

[24] M. M. Glazov, T. Amand, X. Marie, D. Lagarde, L. Bouet, and B. Urbaszek, Exciton fine structure and spin decoherence in monolayers of transition metal dichalcogenides, Phys. Rev. B **89**, 201302(R) (2014).

[25] H. Yu, G.-B. Liu, P. Gong, X. Xu, and W. Yao, Dirac cones and Dirac saddle points of bright excitons in monolayer transition metal dichalcogenides, Nat. Commun. **5**, 3876 (2014).

[26] J. Kim, X. Hong, C. Jin, S.-F. Shi, C.-Y. S. Chang, M.-H. Chiu, L.-J. Li, and F. Wang, Ultrafast generation of pseudo-magnetic field for valley excitons in WSe_2 monolayers, Science **346**, 1205 (2014).

[27] G. Kioseoglou, A. T. Hanbicki, M. Currie, A. L. Friedman, and B. T. Jonker, Optical polarization and intervalley scattering in single layers of MoS_2 and $MoSe_2$, Sci. Rep. **6**, 25041 (2016).

[28] H. Wang, C. Zhang, W. Chan, C. Manolatou, S. Tiwari, and F. Rana, Radiative lifetimes of excitons and trions in monolayers of the metal dichalcogenide MoS_2, Phys. Rev. B **93**, 045407 (2016).

[29] Y. C. Lee, and P. S. Lee, Coherent radiation from thin films, Phys. Rev. B **10**, 344 (1974).

[30] G. Björk, S. Pau, J. Jacobson, and Y. Yamamoto, Wannier exciton superradiance in a quantum-well microcavity, Phys. Rev. B **50**, 17336 (1994).

[31] See Supplemental Material at http://link.aps.org/supplemental/10.1103/PhysRevResearch.4.023168 for which contains additional theoretical description, detailed estimates, as well as a citation to Ref. [48].

[32] H. H. Fang, B. Han, C. Robert, M. A. Semina, D. Lagarde, E. Courtade, T. Taniguchi, K. Watanabe, T. Amand, B. Urbaszek *et al.*, Control of the Exciton Radiative Lifetime in van der Waals Heterostructures, Phys. Rev. Lett. **123**, 067401 (2019)

[33] G. Moody, C. K. Dass, K. Hao, C.-H. Chen, L.-J. Li, A. Singh, K. Tran, G. Clark, X. Xu, G. Berghäuser *et al.*, Intrinsic homogeneous linewidth and broadening mechanisms of excitons in monolayer transition metal dichalcogenides, Nat. Commun. **6**, 8315 (2015).

[34] C. Robert, D. Lagarde, F. Cadiz, G. Wang, B. Lassagne, T. Amand, A. Balocchi, P. Renucci, S. Tongay, B. Urbaszek *et al.*, Exciton radiative lifetime in transition metal dichalcogenide monolayers, Phys. Rev. B **93**, 205423 (2016).

[35] G. Plechinger, P. Nagler, A. Arora, R. Schmidt, A. Chernikov, A. G. del Águila, P. C. M. Christianen, R. Bratschitsch, C. Schüller, and T. Korn, Trion fine structure and coupled spin-valley dynamics in monolayer tungsten disulfide, Nat. Commun. **7**, 12715 (2016).

[36] F. Cadiz, E. Courtade, C. Robert, G. Wang, Y. Shen, H. Cai, T. Taniguchi, K. Watanabe, H. Carrere, D. Lagarde *et al.*, Excitonic Linewidth Approaching the Homogeneous Limit in MoS_2-Based van der Waals Heterostructures, Phys. Rev. X **7**, 021026 (2017).

[37] R. Bonifacio and L. A. Lugiato, Optical bistability and cooperative effects in resonance fluorescence, Phys. Rev. A **18**, 1129 (1978).

[38] S. S. Hassan, P. D. Drummond, and D. F. Walls, Dispersive optical bistability in a ring caivty, Opt. Commun. **27**, 480 (1978).

[39] H. M. Gibbs, S. L. McCall, T. N. C. Venkatesan, A. C. Gossard, A. Passner, and W. Wiegmann, Optical bistability in semiconductors, Appl. Phys. Lett. **35**, 451 (1979).

[40] C. M. Bowden, C. C. Sung, First- and second-order phase transitions in the Dicke model: Relation to optical bistability, Phys. Rev. A **19**, 2392 (1979).

[41] J. A. Hermann and H. J. Carmichael, Stark effect in dispersive optical bistability, Opt. Lett. **7**, 207 (1982).

[42] E. Ginossar, L. S. Bishop, and S. M. Girvin, Nonlinear oscillators and high fidelity qubit state measurement in circuit quantum electrodynamics, in *Fluctuating Nonlinear Oscillators. From nanomechanics to quantum superconducting circuits* (Oxford University Press, 2012).

[43] V. Shahnazaryan, I. Iorsh, I. A. Shelykh, and O. Kyriienko, Exciton-exciton interaction in transition-metal dichalcogenide monolayers, Phys. Rev. B **96**, 115409 (2017).

[44] G. Rochat, C. Ciuti, V. Savona, C. Piermarocchi, A. Quattropani, and P. Schwendimann, Excitonic Bloch equations for a two-dimensional system of interacting excitons, Phys. Rev. B **61**, 13856 (2000).

[45] O. L. Berman, Yu. E. Lozovik, and D. W. Snoke, Theory of Bose-Einstein condensation and superfluidity of two-dimensional polaritons in an in-plane harmonic potential, Phys. Rev. B **77**, 155317 (2008).

[46] S. Mandal, K. Dini, O. V. Kibis, and T. C. H. Liew, On the possibility of a terahertz light emitting diode based on a dressed quantum well, Sci. Rep. **9**, 16320 (2019).

[47] A. Iurov, L. Zhemchuzhna, D. Dahal, G. Gumbs, and D. Huang, Quantum-statistical theory for laser-tuned transport and optical conductivities of dressed electrons in $\alpha - \mathcal{T}_3$ materials, Phys. Rev. B **101**, 035129 (2020).

[48] J. D. Joannopoulos, S. G. Johnson, J. N. Winn, and R. D. Meade, *Photonic Crystals: Molding the Flow of Light* (Princeton University Press, 2008).